

A compact viewing configuration for stereoscopic micro-PIV utilizing mm-sized mirrors

S. M. Hagsäter · C. H. Westergaard ·
H. Bruus · J. P. Kutter

Received: 17 January 2008 / Revised: 29 April 2008 / Accepted: 16 May 2008 / Published online: 20 June 2008
© Springer-Verlag 2008

Abstract When applying PIV to micrometer-resolution systems, the out-of-plane velocity component has shown to be much more difficult to obtain than the two in-plane velocity components. In this work, we present a novel stereoscopic viewing configuration for stereoscopic micro-PIV, utilizing mm-sized mirrors introduced in front of the microscope objective lens. Attractive applications, where the advantage of the mirror viewing configuration system could be utilized, include (on-chip) miniaturization and the potential to introduce more than two simultaneous viewing angles. Here, a first validation of our system is presented, including stereoscopic micro-PIV measurements in a micro-fabricated test device.

1 Introduction

In microfluidic systems the limited optical access poses restrictions to flow velocity measurements. With the micro-PIV technique (Santiago et al. 1998) the two in-plane velocity components can readily be obtained due to the combination of volumetric illumination and focal suppression (Meinhart et al. 2000). However, in many microfluidic scenarios the objective is to quantify a flow of three-dimensional nature, and it is therefore desirable to measure all three velocity components.

In standard PIV, stereoscopic methods have been used for many years by aiming two individual cameras onto the same planar light sheet either with lateral displacement (object plane, lens plane and image plane remain parallel; no distortion is introduced) or angular displacement (the image plane must be tilted according to the Scheimpflug condition (Scheimpflug 1904) in order to maintain focus in the object plane; perspective distortion is introduced) (Prasad and Jensen 1995; Prasad 2000). Angular displacement is the most widely used, since one gains better focusing with normal optics at large viewing angles. The viewing angle between the cameras is best at $2 \times 45^\circ$, because with a right angle the measurement resolution will be the same in all directions. Due to practical limitations, smaller angles are often used, but nevertheless these angles are still relatively large. An alternative solution utilizing lateral displacement was presented by Arroyo and Greated (1991). In their system, a set of mirrors was used to create stereoscopic views, and a single camera was used to record image frames.

Scaling the standard stereo PIV setup down to accommodate microfluidic applications poses the challenges of utilizing volumetric illumination (just as in ordinary micro-PIV), and finding physical room for large aperture light collecting lenses sufficiently close to the microfluidic device, while maintaining a sufficiently large angle between the views. An apparent straightforward solution would be to utilize a stereo microscope. These can be found in two different types: the common main objective type (CMO), which utilizes lateral displacement, and the Greenough type, which basically utilizes angular displacement (the optics are adapted for microscopy eye-viewing purpose, so there is no Scheimpflug correction). The main benefits with the Greenough configuration are the high numerical aperture and the high optical resolution.

S. M. Hagsäter (✉) · H. Bruus · J. P. Kutter
Department of Micro- and Nanotechnology, Technical
University of Denmark, 2800 Kongens Lyngby, Denmark
e-mail: mes@mic.dtu.dk; melker.hagsater@mic.dtu.dk

C. H. Westergaard
Vestas Wind Systems A/S, Frederiksborgvej 399,
4000 Roskilde, Denmark

The main advantages with the more popular CMO configuration are that there is no perspective distortion and that infinity optics are used. The main drawbacks with the CMO configuration are the need for a large front lens and the limited optical magnification readily available.

However, the main limitation of stereoscopic micro-PIV realizations using standard stereo microscopes is in particular the angle between the views, since these microscopes are adapted to the human requirement of a convergence angle of around 10° to 12° . This poses a limitation with respect to the resolution of the out-of-plane velocity components. Successful applications of stereo micro-PIV using stereo microscopes can be found in Klaseen et al. (2005), Lindken et al. (2006) and Bown et al. (2006). An alternative method is demonstrated by Klank et al. (2002). Here, by using the translation method in an ordinary microscope, the 3D flow velocities are obtained by recombining two view angles from a “fly-over” performed in a cartographic manner.

There are also examples of other non-stereoscopic particle-based velocimetry techniques, with which it is feasible to derive the out-of-plane flow components in microfluidic systems. Some recent publications include: deconvolution microscopy (Park and Kihm 2006), holographic methods (Satake et al. 2006), optically sliced methods (Kinoshita et al. 2007), and continuity based techniques (Bown et al. 2007). However, the working principles and validation of these methods will not be subject to further discussion in this manuscript.

In the stereoscopic micro-PIV realization presented in this paper, the single optical path of an upright research microscope is utilized. The two respective inclined views are achieved by placing a set of mm-sized mirrors (coated glass prisms) between the sample to be investigated and the microscope objective front lens. One advantage of this setup is the high level of adaptability that it provides. For instance, the angle between the views can be made larger than what is typically given by a stereo microscope lens, which is a limiting factor for the accuracy of the stereoscopic micro-PIV method.

An additional benefit is the potential to include the splitter mirror system directly in contact with or as a part of the microfluidic system (Chronis and Lee 2004). This would allow routine inspections to be performed at defined positions, using a standard microscope. Such a system would greatly benefit from miniaturized mirror sets, allowing for higher magnification objectives to be used. Alternatively to the previous solution, the splitter system could be integrated with the front lens of the microscope objective. Such a configuration would allow free in-plane translational movement of the substrate, thus readily allowing multiple points of inspection. Other benefits would be the simpler handling, including no requirement

for pre-alignment of the mirrors, less clutter of workspace and the ability to perform faster calibrations. Finally, by expanding the same principal design, a mirror system allowing more than two views is feasible. Such a system could be utilized in a first realization of tomographic micro-PIV.

The potential of a viewing configuration utilizing mm-sized mirrors is demonstrated in two experimental setups. First, by an in-air example where the displacement of immobilized micro-particles is measured. And, secondly, through an investigation of the flow over a step in a microfluidic channel.

2 Materials and methods

2.1 Experimental setup

The central component of the experimental setup used in this study is the mirroring system, placed between the front lens of the microscope objective and the sample. It consists of three custom-made glass prisms with reflecting coatings that are aligned with respect to each other, as shown in Fig. 1. With this arrangement, two separate views from different angles will be obtained. To facilitate the alignment of the mirrors a special holder was designed (see Fig. 2), in which the central prism is held in place above a 6×6 mm square hole in the 2 mm thick holder substrate. The two side prisms are positioned in the 10 mm wide carved tracks extending horizontally from the central prism. The holder was in turn placed onto a 2 mm thick lever (not shown here), extending from a translational stage, which allowed the mirror system to be fine-positioned between the microscope objective and the sample.

Images were recorded with a HiSense MkII CCD camera (Dantec Dynamics), mounted with a $0.63 \times$ TV-adaptor on a research microscope (Leica DMLB). The mirror system was designed to be used with a $5\times$ magnification objective (N Plan, Leica), with a numerical aperture, NA, of 0.12. With this combination, the total magnification was $3.15\times$, providing a field of view of 2.1×2.8 mm.

The samples were illuminated from below by two light emitting diodes (Luxeon Star 3W, Lumileds), mounted with plastic focusing lenses (FFLI, Fraen Srl) (Hagsäter et al. 2008). The LEDs were controlled by a PIV timing system (Dantec Dynamics) and powered by an in-house built power supply, allowing the light pulses to be synchronized individually with the camera. The diodes were positioned manually with the tip of the lenses ~ 25 mm apart, and at a distance ~ 35 mm below the level of the microscope's translational stage. When fluorescent signal was recorded, a short pass filter (500 nm, Thorlabs), was

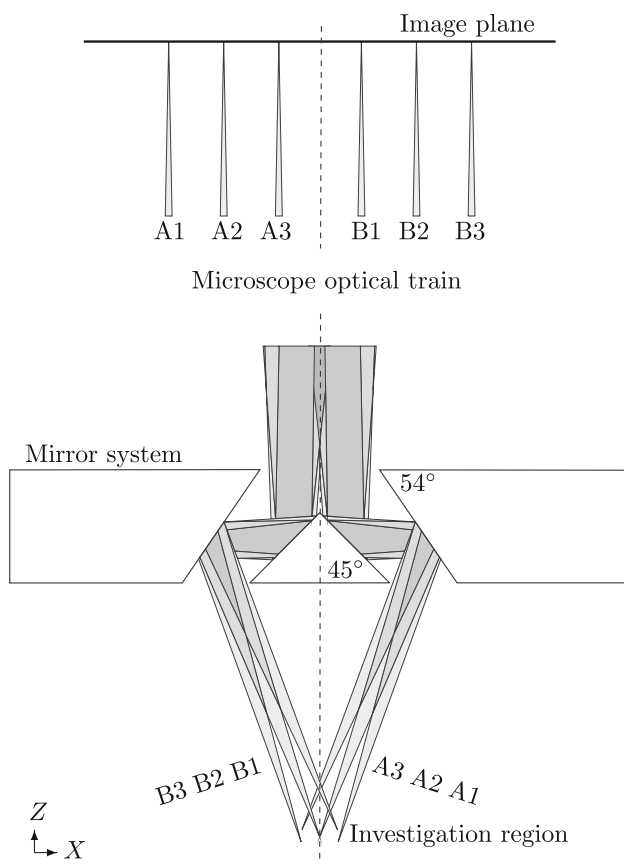


Fig. 1 Ray-tracing through the mirroring system used in the experiments. The height of the central prism is 1.5 mm providing a top angle of 90° , whereas the side mirrors are designed with a 54° degree angle, as shown in the figure. The ray-bundles $A1$ – $A3$ and $B1$ – $B3$ show how the inclined views in the investigation region will be positioned in relation to each other at the image plane (as viewed by the CCD). Note that the ray-paths cross over in the microscope

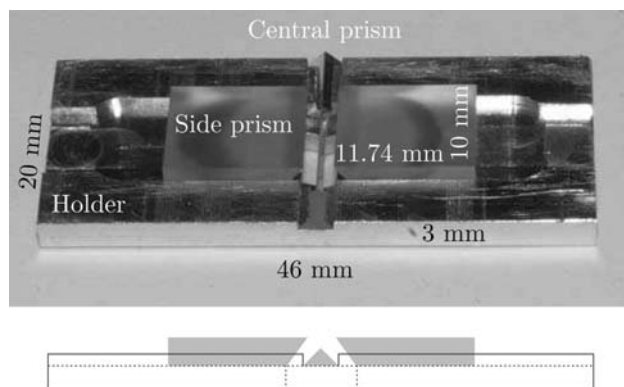


Fig. 2 *Top panel* shows a picture of the holder with the prisms inserted. The central prism, 20 mm wide, is fixed in position in the middle of the holder. The side prisms, 10 mm wide, can be moved back and forth along the 10 mm wide and 1 mm deep tracks. There is a square hole (6×6 mm) in the center of the holder, which, in the figure, is covered by the mirrors. *Bottom panel* shows a sketch of the arrangement as seen from the side

positioned between the LEDs and the microfluidic chip, and an I3 filter cube (Leica) was inserted in the filter turret. In the flow measurements, green fluorescent polystyrene particles ($5 \mu\text{m}$ diameter, Duke Scientific), were used to trace the flow. For the in-air measurements, the same $5 \mu\text{m}$ polystyrene beads were immobilized in epoxy resin, and spread out in a thin layer onto a glass wafer.

The calibration targets were defined through UV-lithography of positive photo-resist spun on top of a $500 \mu\text{m}$ thick pyrex glass wafer. They consisted of 5×11 dots, $100 \mu\text{m}$ wide, equally spaced $200 \mu\text{m}$ center-to-center. An origin was defined by making the centermost dot larger ($150 \mu\text{m}$ wide), and enclosing it with four smaller dots ($75 \mu\text{m}$ wide). The same type of target was used for both the in-air measurements and the micro-chip flow measurements.

The flow measurements were performed in a microfluidic chip, consisting of a rectangular channel manufactured through welding of glass pieces (channel dimensions $1 \times 14 \times 48$ mm). The ridge (dimensions $0.5 \times 14 \times 10$ mm) and the target (height $\sim 700 \mu\text{m}$) were positioned manually into the channel, which afterwards was sealed with a $\sim 140 \mu\text{m}$ thick glass lid.

The image acquisitions, image manipulations, 3D-calibrations and calculations were all performed on a PC with Flowmanager software (Dantec Dynamics).

2.2 Stereoscopic calibration and the “no Scheimpflug” condition

For the measurements presented in this paper, the stereoscopic calibration was performed in the same way as in a macroscopic PIV system using a calibration target and a translation stage, taking pictures at five different levels of depth. For these initial studies a direct linear transform as explained in Willert (1997) was used for the mapping between the investigation region and the image plane (CCD). The implementation is documented in the software manual for the program Flowmanager (Dantec Dynamics). An example of a recorded image frame, showing the calibration target from the two respective views (at $Z = 0$) is shown in Fig. 3 (see figure caption for additional information). As shown in the figure, the two views are recorded onto the same image frame.

For the in-air calibrations, the calibration target was traversed step-wise in the vertical direction, from -100 to $100 \mu\text{m}$. To achieve a correct calibration in water, the calibration target’s position inside the microchannel should be adjusted. This is to account for the difference in refractive index between water and air. However, this approach was not feasible using the current test structure, where the calibration target was locked in its position. Instead, the calibration was performed in a similar way as

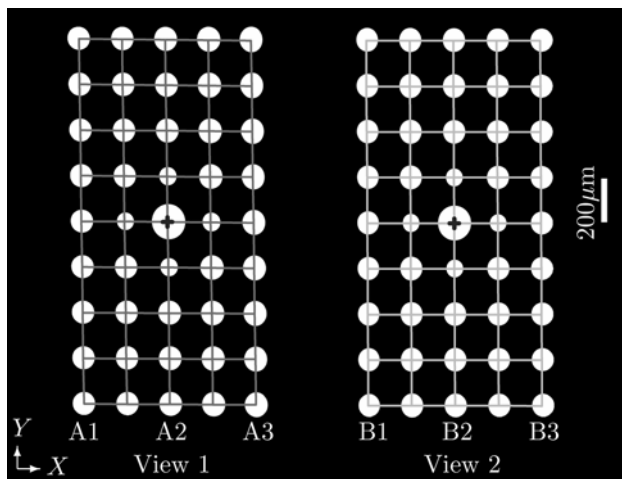


Fig. 3 Recorded image frame (transformed into a binary image by contrast enhancement) showing the calibration target from the two respective angular views. $A1$ – $A3$ and $B1$ – $B3$ correspond to the same notations as in the cross-sectional view in Fig. 1. Grid-nets showing the linear transform are superimposed on top of the dots (view 1, dark gray and view 2, bright gray) and the common origin is indicated by the ‘+’-marks

for the in-air calibration, but here the whole microchip (filled with water) was traversed step-wise between Z values of -100 to $100 \mu\text{m}$. This gives an adequately correct calibration in the X and Y directions, but the Z direction is wrong by the depth magnification in water. This was compensated for in the software by multiplying the actual vertical displacements with the refractive index of water (1.33), corresponding to step-wise displacements of $\pm 133 \mu\text{m}$, as if the target had been moved inside the water filled channel. This was found to be a sufficient enough approach for this first feasibility study of our stereoscopic viewing configuration, but since this calibration method has clear limitations as to its applicability for the investigation of lab-on-a-chip systems, other calibrations methods (Wieneke 2005) are generally recommended. The splitting mirror system was held in a fixed position with respect to the microscope objective, and the target plate was moved with the microscope’s focusing translation stage. The central calibration position ($Z = 0$) was chosen so that the middle column of dots on the calibration target was in focus in both views.

When the target is traversed in the vertical direction, the dots’ in-plane positions are shifted (in the image plane). For the in-air measurements, a movement of $6.75 \mu\text{m}$ in Z was found to result in a one pixel in-plane displacement. Since the in-plane resolution is $2.0 \mu\text{m}$ per pixel, this corresponds to a depth resolution of roughly $1/3$ of the in-plane resolution, or an angle between the views of $\sim 34^\circ$. For the measurements in the micro-chip, the calibration was performed similarly, with a movement of $8.9 \mu\text{m}$ in Z resulting in a one pixel in-plane displacement. Due to the

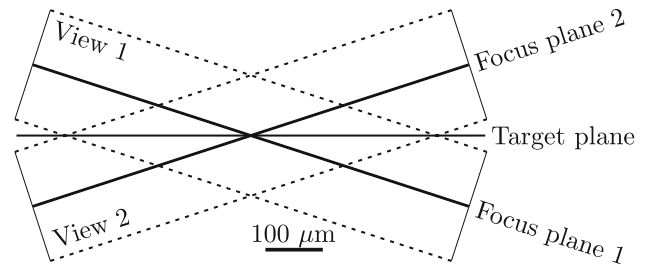


Fig. 4 A cross-sectional view of how the focus planes are located for the two respective angular views. In the figure, the displacement of the focus planes with respect to the target plane, $\pm 17^\circ$, is given for inspection in air using the current setup. The depth of focus is indicated by the dashed lines, here drawn with a $\pm 100 \mu\text{m}$ separation from the focus planes

air-glass-water transition, here the angle between the two views was found to be $\sim 26^\circ$, which corresponds to a depth resolution of about $1/4$ of the in-plane resolution.

In a classical setup, where two cameras are used for recording stereoscopic views, the Scheimpflug condition (Scheimpflug 1904) can be satisfied by tilting the cameras’ image planes (the CCDs) according to the object plane. However, the stereoscopic viewing configuration described here has not yet been accommodated to include multiple CCDs; so far, only a single CCD has been used. Thus, with respect to a flat target, or a common measurement plane, the two focus planes will be tilted according to the viewing angles (see Fig. 4). This is a clear limitation of the current setup, but not a drawback of the single optical path configurations as such, and suggestions on designs that circumvent this limitation are discussed further below.

3 Results

3.1 Displacement measurements conducted in air

As a first validation of the method, displacement measurements of immobilized particles (conducted in air) were performed. For this experiment, the $5 \mu\text{m}$ polystyrene beads were mixed with epoxy resin, and thereafter spread out in a thin layer onto a diced pyrex glass wafer of the same thickness as the calibration target. Double-image frames were composed from single frames, where the microscope’s translational stage was used to displace the particles (in one of the directions, X , Y or Z) between the two recordings. The results from these displacement measurements are seen in Fig. 5. Qualitatively, no displacement in Z is measured for translations in-plane, and, contrariwise, no in-plane displacements are measured for the translation in Z . This is the most important result of this experiment, as it shows that the proposed stereoscopic micro-PIV approach is capable of separating displacements

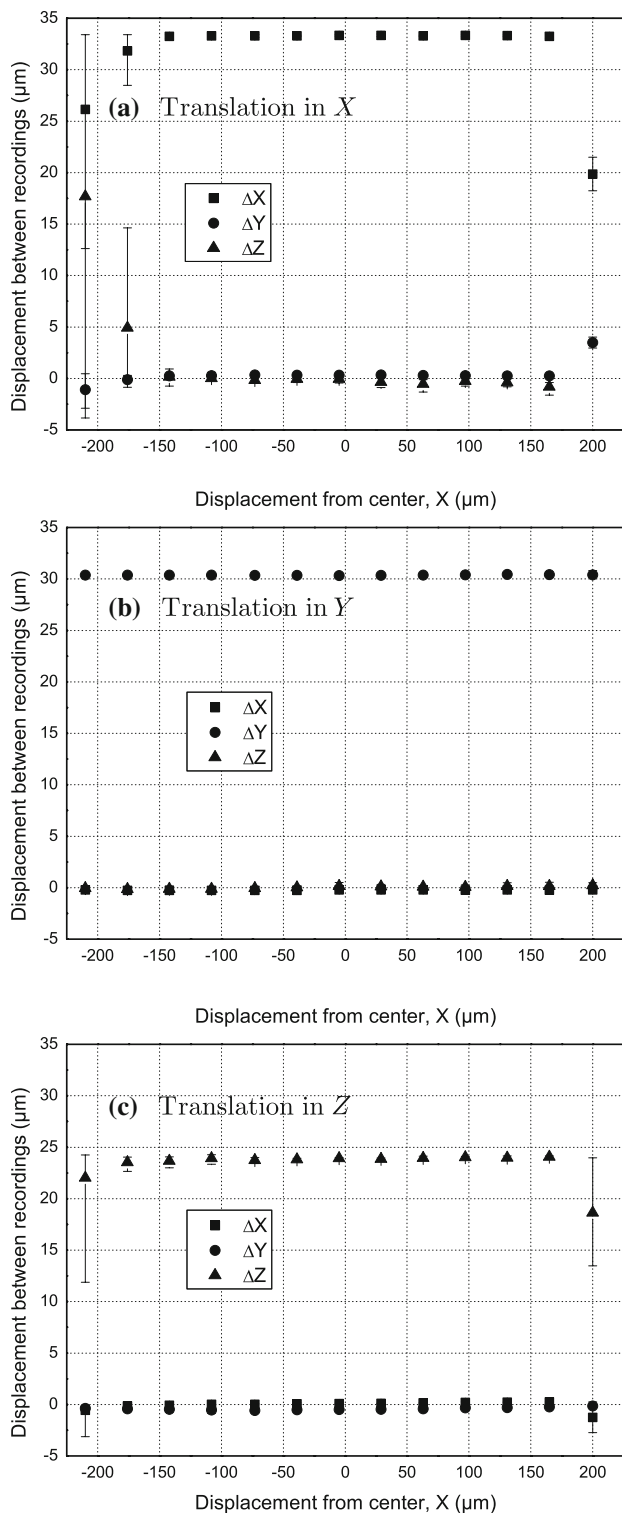


Fig. 5 The measured displacement of translations (a) $\sim 33 \mu\text{m}$ in X , (b) $\sim 30 \mu\text{m}$ in Y and (c) $\sim 24 \mu\text{m}$ in Z , respectively. The interrogation area used was 64×64 pixels, with a $75 \times 50\%$ overlap. Displayed is the average of the 10 middle vectors for each column, with *error bars* showing the min and max values within each data set. For larger displacements from the center, due to the no Scheimpflug condition, there is not enough overlap between the two views to produce valid vectors

in three dimensions. Due to the fact that all the particles are located within a thin sheet, and given the relatively large depth of focus of the system, homogeneous displacements are measured for a fairly large part of the image field ($\pm 150 \mu\text{m}$ in-plane from the intersection). However, for larger distances from the intersection, due to the lack of overlap between the two views, the displacements could not be quantified.

3.2 Measurement of flow over a micro-step

In the next experiment, the flow over an upwards step in a micro-channel was measured. Here, the addition of volume illumination further restrains the workable measurement region of the current one-CCD system. Nonetheless, we are able to obtain valid 3D velocity data in a common region around the center, where the focus planes for the two views have a large overlap (as was shown in Fig. 4). The system was calibrated with the calibration target positioned inside the micro-channel (which was filled with water during the calibration) and thereafter, the stage was traversed (15 mm) in-plane to the position of the step. Measurements were performed in three partly overlapping positions: directly over the step, and approximately ± 1 mm upstream and downstream with respect to the middle position, as shown in Fig. 6a–c. All three measurements were performed in the center of the channel (total width 14 mm) in consecutive order. For measurements in water, with $5 \mu\text{m}$ particles, the depth of correlation (Olsen and Adrian 2000) is about $200 \mu\text{m}$. Double image frames with a time separation of 30 ms were recorded in fluorescent mode (Hagsäter et al. 2008) using LED illumination pulses of 2 ms. Velocity vectors were calculated using adaptive correlation with an interrogation area of 64×64 and an overlap of 50%. For each position 100 double images were used for averaging.

The measured velocity V was $\sim 125 \mu\text{m/s}$ upstream and $\sim 300 \mu\text{m/s}$ downstream of the step. The out of plane velocity W was close to zero, except for just before the step, where the measurement indicated the presence of an upward flow (see Fig. 6b). Finally, the velocity U , perpendicular to the main flow direction V was close to zero through the investigated region. The measured velocities were validated by comparison with calculated velocities for a 2D-cross sectional model, using COMSOL finite element method software (displayed as lines in Fig. 6). This comparison showed a good agreement between the two.

4 Discussion

With the two experimental test examples, we have demonstrated the capability of the stereoscopic viewing

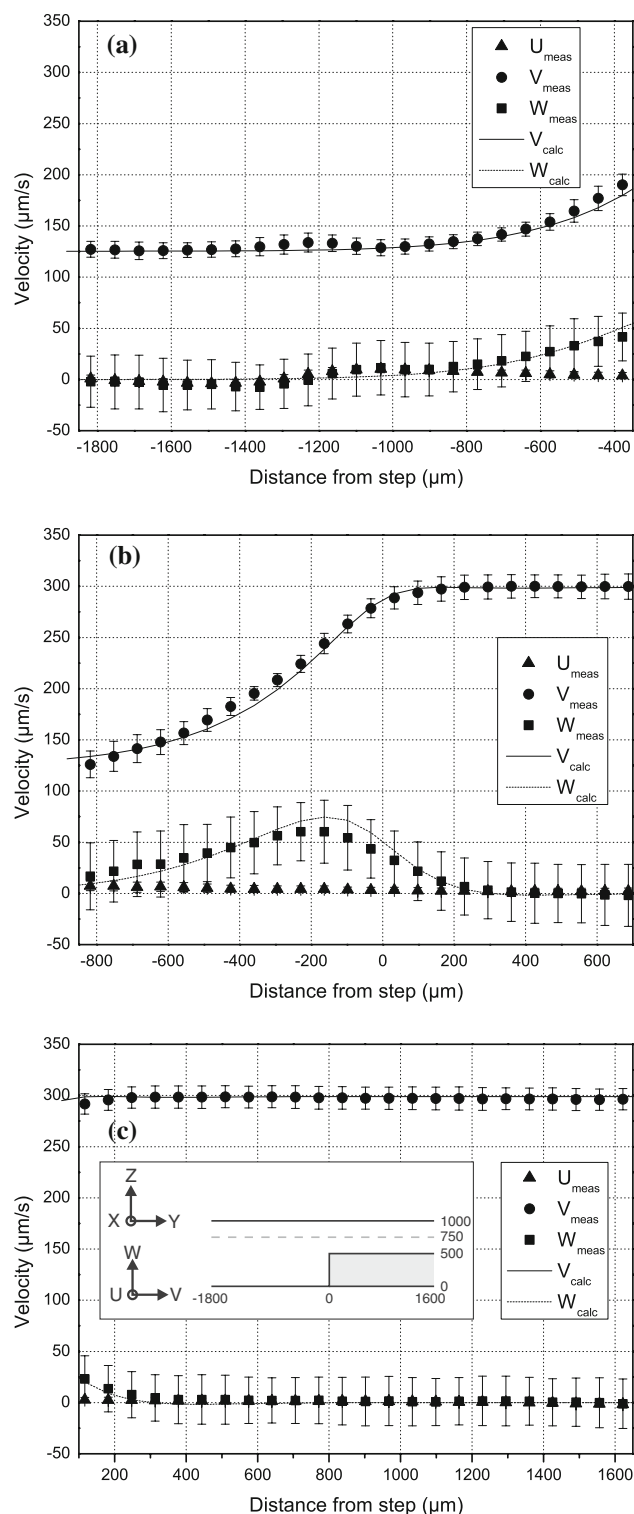


Fig. 6 Measured (dots) and calculated (lines) velocities of the flow (a) upstream, (b) above, and (c) downstream of a step in a micro-channel. The error-bars are showing the standard-deviation, which, as expected from the angle between the views being smaller than 45° , is larger for the in-depth velocity component W than for the in-plane velocity components U and V . The calculated velocities are displayed for a height of $750\ \mu\text{m}$ from the model's bottom boundary wall. This depth was chosen to fit with the measured velocity V

configuration for reliable 3D velocity measurements. In the current realization a magnification of $3.15\times$ was used, corresponding to a total field of view of two times $2.1 \times 1.4\ \text{mm}$. In practice, however, because the current realization does not fulfill the Scheimpflug condition, the measurements were limited to be performed in the vicinity of the common optical axis only. Nonetheless, this should not be interpreted as a general limitation of the single optical axis stereo viewing principle as such. By adjusting the angles and the position of the mirrors it is possible to create a larger separation between the views in the image plane, which in turn would allow the views to be captured by individual CCDs. Alternatively, the two views could be separated perpendicularly to the microscope's principal axis by fitting additional splitting mirrors in the optical train, after the tube lens (more complex solutions including glass materials or lenses could also be imagined). However, these further developments towards a more complete system are beyond the scope of this study, where the main focus has been on the components placed in between the sample of investigation and the microscope's objective.

Another line of investigation for the future would be to shrink the mirror setup to fit to higher magnification systems. With the current realization, it should be possible to make a model to fit to, at least, a $10\times$ magnification, though it would require some modifications with respect to the alignment and handling of the system. Naturally, the increased resolution by itself would be an improvement, but the true objective would be to investigate how to incorporate stereoscopic viewing ability during the fabrication or packaging of micro-devices, utilizing the same stereoscopic viewing principle as proposed in this manuscript. This would allow routine inspection to be performed at defined positions, using a standard microscope. An alternative for future studies would be to inquire into an integration of the splitter system directly with the front lens of the microscope objective. Such a configuration would facilitate handling, and would be practical for multiple points of inspection, or scanning, experiments. A final suggestion for future applications would be to expand the same principal design to include more than two views. Such a system could then be utilized as a first realization of tomographic micro-PIV.

It should also be mentioned that there are other ways in which our system could be improved, more related to the implementation of the stereoscopic micro-PIV method. For instance, one way to increase the accuracy is by introducing a pre-processing procedure to remove invalid particles, i.e., particles that are only appearing (in focus) in one of the views (Bown et al. 2006). Furthermore, the calibration procedure used in this study is not practical for most microfluidic applications, but there are examples of

other calibration procedures, which we propose to implement (Wieneke 2005).

5 Conclusions

We have successfully demonstrated the functionality of the optical setup and shown that reliable result can be obtained. The current system still has a number of shortcomings, where first and foremost the system does not fulfill the Scheimpflug condition. However, we have several suggestions on how to engineer a solution to this limitation. Other potential improvements include mirrors designed to be used with higher magnification objectives, further increase of the angle between the views and realizations with stereoscopic viewing incorporated on-chip.

Acknowledgments SMH was supported through Copenhagen Graduate School for Nanoscience and Nanotechnology, in a collaboration between Dantec Dynamics A/S and DTU Nanotech, the Department of Micro- and Nanotechnology.

References

- Arroyo MP, Greated CA (1991) Stereoscopic particle image velocimetry. *Meas Sci Technol* 2(12):1181–1186
- Bown MR, MacInnes JM, Allen RWK, Zimmerman WBJ (2006) Three-dimensional, three-component velocity measurements using stereoscopic micro-PIV and PTV. *Meas Sci Technol* 17(8):2175–2185
- Bown MR, MacInnes JM, Allen RWK (2007) Three-component micro-PIV using the continuity equation and a comparison of the performance with that of stereoscopic measurements. *Exp Fluids* 42(2):197–205
- Chronis N, Lee LP (2004) Total internal reflection-based biochip utilizing a polymer-filled cavity with a micromirror sidewall. *Lab Chip* 4(2):125–130
- Hagsäter SM, Westergaard CH, Bruus H, Kutter JP (2008) Investigations on LED illumination for micro-PIV including a novel front-lit configuration. *Exp Fluids* 44:211–219
- Kinoshita H, Kaneda S, Fujii T, Oshima M (2007) Three-dimensional measurement and visualization of internal flow of a moving droplet using confocal micro-PIV. *Lab Chip* 7(3):338–346
- Klank H, Goranovic G, Kutter JP, Gjelstrup H, Michelsen J, Westergaard CH (2002) PIV measurements in a microfluidic 3D-sheathing structure with three-dimensional flow behaviour. *J Micromech Microeng* 12(6):862–869
- Klasen LG, Leder A, Brede M (2005) Entwicklung und Aufbau eines Stereo-Mikro-PIV System zur instantanen Strömungsfeldmessung. In: *Lasermethoden in der Strömungsmesstechnik - 13. Fachtagung der GALA e.V. 2005*, GALA e.V., BTU Cottbus, S. 9.1–9.8
- Lindken R, Westerweel J, Wieneke B (2006) Stereoscopic micro particle image velocimetry. *Exp Fluids* 41(2):161–171
- Meinhart CD, Wereley ST, Gray MHB (2000) Volume illumination for two-dimensional particle image velocimetry. *Meas Sci Technol* 11(6):809–814
- Olsen MG, Adrian RJ (2000) Out-of-focus effects on particle image visibility and correlation in microscopic particle image velocimetry. *Exp Fluids* 29(7):166–174
- Park JS, Kihm KD (2006) Three-dimensional micro-PTV using deconvolution microscopy. *Exp Fluids* 40(3):491–499
- Prasad AK (2000) Stereoscopic particle image velocimetry. *Exp Fluids* 29(2):103–116
- Prasad AK, Jensen K (1995) Scheimpflug stereocamera for particle image velocimetry in liquid flows. *Appl Opt* 34(30):7092–7099
- Santiago JG, Wereley ST, Meinhart CD, Beebe DJ, Adrian RJ (1998) A particle image velocimetry system for microfluidics. *Exp Fluids* 25(4):316–319
- Satake S, Kunugi T, Sato K, Ito T, Kanamori H, Taniguchi J (2006) Measurements of 3D flow in a micro-pipe via micro digital holographic particle tracking velocimetry. *Meas Sci Technol* 17(7):1647–1651
- Scheimpflug T (1904) Improved method and apparatus for the systematic alteration or distortion of plane pictures and images by means of lenses and mirrors for photography and for other purposes. GB Patent No. 1196
- Wieneke B (2005) Stereo-PIV using self-calibration on particle images. *Exp Fluids* 39(2):267–280
- Willert C (1997) Stereoscopic digital particle image velocimetry for application in wind tunnel flows. *Meas Sci Technol* 8(12):1465–1479